

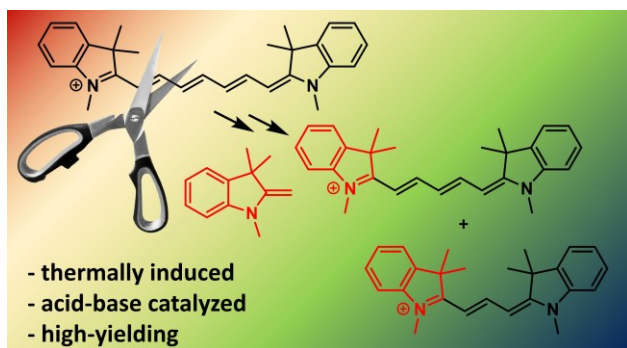
Thermal Truncation of Heptamethine Cyanine Dyes

Jana Okoročenkova,^{†,‡} Josef Filgas,[¶] Nasrulla Majid Khan,^{†,‡} Petr Slavíček,^{¶,*} Petr Klán^{†,‡,*}

[†] Department of Chemistry, Faculty of Science, Masaryk University, Kamenice 5, 625 00, Brno, Czech Republic.

[‡] RECETOX, Faculty of Science, Masaryk University, Kamenice 5, 625 00, Brno, Czech Republic.

[¶] Department of Physical Chemistry, University of Chemistry and Technology, Technická 5, 16628 Prague 6, Czech Republic.



ABSTRACT: Cyanine dyes are a class of organic, usually cationic molecules containing two nitrogen centers linked through conjugated polymethine chains. Unlike phototruncation, the thermal truncation (chain-shortening) reaction is a phenomenon that has rarely been described for these important fluorophores. Here, we present a systematic investigation of the truncation of heptamethine cyanines (Cy7) to pentamethine (Cy5) and trimethine (Cy3) cyanines via homogeneous, acid-base catalyzed nucleophilic exchange reactions. We demonstrate how different substituents at the C3' and C4' positions of the chain and different heterocyclic end groups, the presence of different bases, nucleophiles and oxygen, solvent properties, and temperature affect the truncation process. The mechanism of chain shortening, studied by various analytical and spectroscopic techniques, was verified by extensive *ab initio* calculation, demonstrating the need to model catalytic reactions by highly correlated wavefunction-based methods. We show that entropic effects control the course of this process. The study provides a critical insight into the reactivity of the polyene chains of cyanines and offers new approaches to the synthesis of *meso*-substituted symmetrical and unsymmetrical pentamethine cyanines from Cy7 derivatives.

Introduction

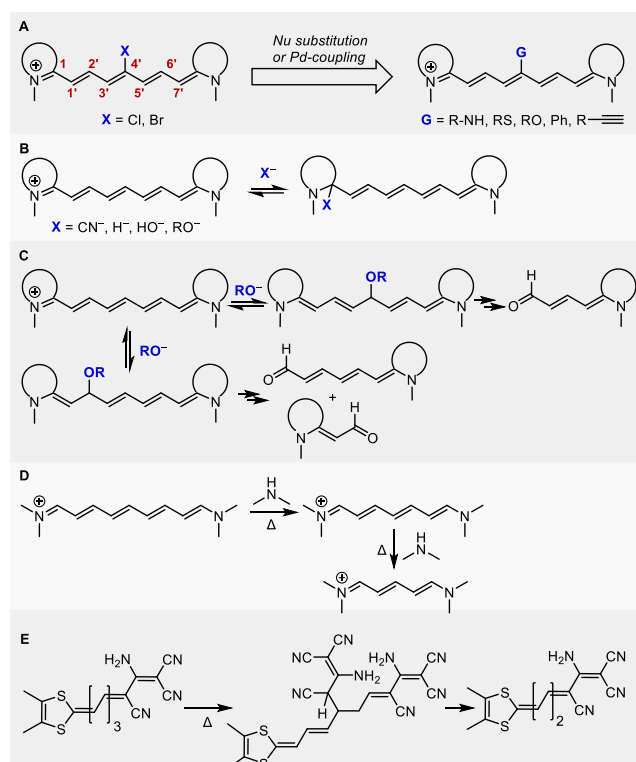
Cyanine dyes have found widespread use as fluorescent probes for labeling nucleic acids and proteins and as photosensitizers in photodynamic therapy, biosensors, and imaging agents.¹⁻⁴ For example, near-infrared fluorescent pentamethine (Cy5) and heptamethine (Cy7) cyanine dyes have emerged as a promising tool for cancer imaging and targeted therapy.⁵⁻⁶ Changing the structures and thus physicochemical properties of Cy5 derivatives affect biodistribution, allowing tissue-specific targeting.⁷⁻⁸ Synthetic strategies toward the modification of cyanines generally rely on an early-stage introduction of various functional groups into the heterocyclic terminal groups or the heptamethine chain.⁹⁻¹²

Further synthetic modifications of cyanines, especially on their polyene chains, is a poorly explored area. Common strategies in Cy7 dyes involve the modification of the chain *meso* position by nucleophilic substitution of the C4'-chloro substituents by N, S, and O nucleophiles via an $S_{RN}1$ reaction¹³⁻¹⁶ or Pd-catalyzed Suzuki¹⁷ or Sonogashira¹⁰ coupling

reactions (Scheme 1A). Due to a positive charge delocalization along the conjugated π -system, hydroxide,¹⁸ alkoxide,¹⁸ cyano,¹⁹⁻²¹ and hydride²² ions can reversibly attack the iminium C1 atom (Scheme 1B). The latter two processes have been utilized in the biosensing of cyanide anions¹⁹⁻²¹ and reactive oxygen species (ROS).²² Few studies reported the addition of hydroxide or alkoxide to the alternating polyene double bonds,^{18,23} such as the methoxide addition to the C2' or C4' chain position of Cy7 or Cy5, followed by spontaneous oxidative fragmentation to aldehydes in aerated solutions (Scheme 1C).²³ It was also demonstrated that the aminolysis of nonamethinecyanines (Cy9) by secondary amines leads to the chain shortening (truncation) to give cyanines Cy7 that subsequently degrade to Cy5 derivatives when treated with amines for a longer time (Scheme 1D).²⁴ Similarly, unexpected chain shortening during the preparation of merocyanine dyes was observed via the attack of a C-nucleophile (Scheme 1E).²⁵⁻²⁶ The polyene chain shortening products were also occasionally observed as side-products during the synthesis of polymethine derivatives;²⁷⁻²⁸ however, the reactions have never been systematically studied.

In conjunction with applications of cyanine dyes in optical imaging and photochemical drug delivery,^{2, 29-31} Schnermann and co-workers described that excitation of Cy7 can also lead to the formation of truncated cyanine derivatives (Cy5), involving a singlet oxygen-initiated multi-step process.³²⁻³⁴ Because the absorption maxima of truncated products are hypsochromically shifted,³⁵⁻³⁶ the photo-truncation reaction is termed *photoblueing*. The photoconversion of Cy5 to Cy3 has also been reported.³⁷

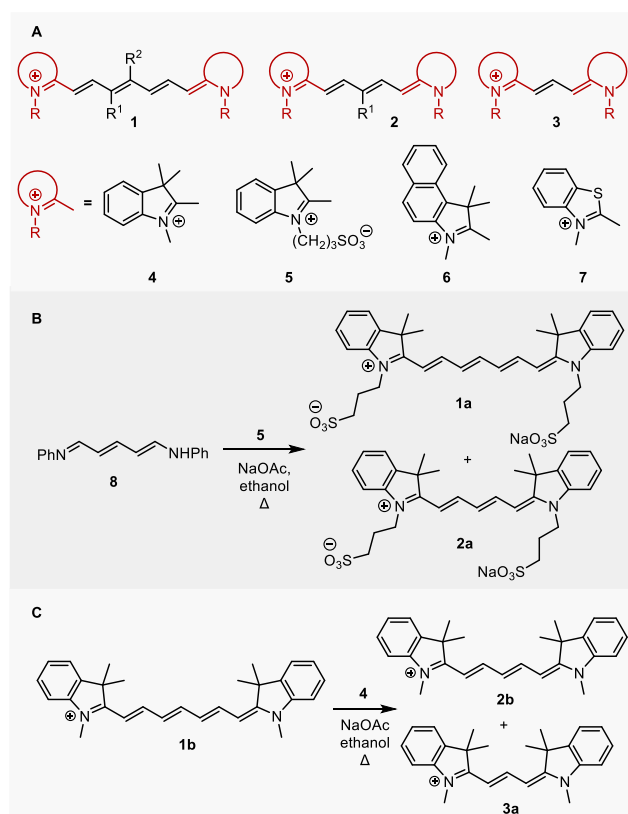
Scheme 1. Reported reactions of polymethine chains with nucleophiles: (a) nucleophilic substitution of halogen atoms or Pd-coupling reactions, (b) reversible addition of nucleophiles to the iminium C1 atom, (c) addition of methoxide to the C2' or C4' chain positions with subsequent fragmentation, (d) aminolysis of polymethine chain resulting in the truncation, (e) the truncation of merocyanines in the presence of a nucleophile.



As a part of our initial investigations of cyanine dyes (general structures **1–3** refer to heptamethine, pentamethine, and trimethine cyanines, respectively, that bear diverse heterocyclic ends **4–7**),¹¹ we initially aimed to prepare a series of chain-substituted Cy7s to examine their physico-chemical properties (Scheme 2A). However, during the preparation of **1a** from [5-(phenylimino)pent-1,3-dien-1-yl]aniline **8** and indolinium salt **5** in the presence of sodium acetate in ethanol,³⁸⁻⁴⁰ we noticed the formation of pentamethine cyanine **2a** with a truncated methine chain as an unexpected side product (Scheme 2B, Figures S4–S6, S39). Truncated polyene products were also obtained by heating Cy7 **1b** in the presence of indolinium salt **4** and sodium acetate in ethanol (Scheme 2C, Figures S7 and S8). These results encouraged us to explore the thermal chain-shortening reactions of cyanines. We studied how different substituents at the C3' and C4' chain positions, different end

heterocycles, the presence of bases, nucleophiles and oxygen, solvent properties, and temperature affect the truncation process of Cy7 dyes. UV-vis spectroscopy, high-performance liquid chromatography (HPLC), high-resolution mass spectrometry (HRMS), nuclear magnetic resonance (NMR) analyses, and quantum chemical calculations were used to create an overall mechanistic picture. Coincidentally, we have become aware of an excellent work by the team of Babak Borhan and James E. Jackson (Michigan State University), which describes a very similar discovery of cyanine thermal truncation and is being submitted at the same time as our paper.

Scheme 2. (a) Cyanines used in the present study; (b) unexpected formation of a Cy5 product **2a observed during the synthesis of **1a**; (c) formation of Cy5 and Cy3 products during heating of heptamethine cyanine **1b** in the presence of indolinium salt **4** and sodium acetate.**



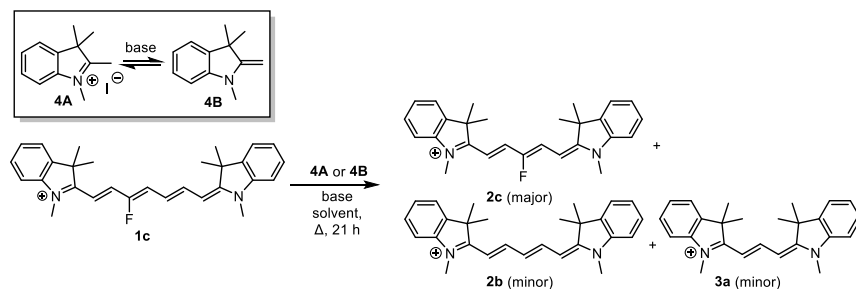
Results and Discussion

Effects of Base, Solvent, Temperature, and Stoichiometry. To evaluate the scope of the truncation reaction, we prepared heptamethine cyanine **1c** (Table 1) on a multi-gram scale from 3-fluoropyridinium salt and indolinium iodide according to the previously published procedures,¹¹⁻¹² which was chosen because it bears an unsymmetrically placed C3'-fluorine atom of the heptamethine chain. It allowed us to identify which part of the chain remains in the truncated product(s). The effects of a solvent (polar protic ethanol or methanol vs. aprotic acetonitrile), base, and temperature on the reaction of **1c** heated with indolinium iodide **4a**, that is, the acid form of **4**, are summarized in Table

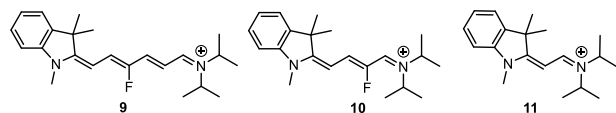
1. Cy7s generally showed better solubility in acetonitrile than in methanol; bases such as NaOAc, *t*-BuOK, or MeONa were well soluble only in ethanol. The corresponding reaction mixture was continuously stirred and heated at 50 or 80°C for 21 h. Careful analyses of the reaction mixture

(HPLC, HRMS, NMR) revealed that 3'-fluoropentamethine cyanine **2c** is always the major product, whereas Cy3 (**3a**; <2%) and non-substituted Cy5 **2b** (<2%) were formed in negligible amounts.

Table 1. Effects of a Base, Solvent, Temperature, Oxygen, and Water ^a



trace hemicyanine intermediates (tentative structures proposed based on HRMS):



solvent	<i>T</i> / °C	4A or 4B (equiv)	base (equiv)	conversion of 1c /%	yield of 2c /% ^b	yield of 3a /%
EtOH	80	4A (2.5)	DBU (5)	75	5	1
EtOH	80	4A (2.5)	NaOAc (5)	>99	22	1
EtOH	80	4A (2.5)	DIPEA (5)	>99	28	2
EtOH	80	4A (2.5)	DIPA (5)	>99	30	2
ACN	80	4A (2.5)	DIPA (5)	>99	33	2
ACN	50	4A (2.5)	piperidine (5)	98	37	1
ACN	50	4A (2.5)	DIPA (5)	96	38	1
ACN	20	4A (2.5)	DIPA (5)	45	10	2
ACN	50	4A (2.5)	–	18	0	0
ACN	50	4A (1)	DIPA (1)	30	6	1
ACN ^c	50	4A (1)	DIPA (2.5)	96	40	2
ACN ^d	50	4A (1)	DIPA (2.5)	97	48	2
ACN	50	4A (1)	DIPA (5)	93	40	1
ACN	50	4A (5)	DIPA (5)	93	24	1
ACN	80	–	DIPA (5)	>99	8	0
ACN	80	–	DIPEA (5)	>99	7	0
ACN	50	4B (1)	–	51	6	2
ACN	80	4B (10)	–	95	31	5
ACN	50	4B (1)	DIPA (2.5)	89	38	1
MeOH	50	4A (1)	<i>t</i> -BuOK (2.5)	72	8	1
MeOH	50	4A (1)	MeONa (2.5)	40	4	1
MeOH	50	4A (1)	pyridine (2.5)	<1	0	0

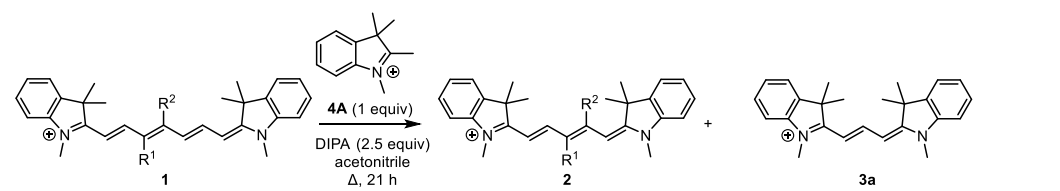
^a [**1c**] = 72 mM, reaction time = 21 h, iodide as a counteranion is omitted for clarity; ACN = acetonitrile. The standard deviation from 5 independent measurements was below 2%. ^b HPLC yields (determined using authentic standards; calculated assuming 100% conversion of **1c**). ^c Degassed with a freeze-pump-thaw method. ^d Dry (anhydrous) acetonitrile, freshly distilled DIPA; degassed with a freeze-pump-thaw method in a glovebox.

Because the sum of chemical yields at complete conversion was always below 50%, we concluded that other degradation pathways were responsible for the mass loss. Indeed, trace amounts of hemicyanines **9**, **10**, and **11**, the adducts of diisopropylamine (DIPA) and cyanine subunits detected in acetonitrile under different reaction conditions, whose structures were proposed from the HRMS data (Figure S12), represent some of possible reaction intermediates or side-products. The stoichiometric amounts of a base, such as sodium acetate, *N,N*-diisopropylethylamine (DIPEA), or DIPA, and a higher temperature (≥ 50 °C) were found indispensable for high truncation yields (up to ~50% of **2c** in both solvents). In contrast, the addition of 1,8-diazabicycloundec-7-ene (DBU) as a non-nucleophilic base provided very low **2c** yields despite a high reaction conversion. Using strong bases, such as *t*-BuOK and MeONa, significantly decreased the **2c** yields. Pyridine as a weak base ($pK_a = 5.2$) did not mediate any reaction. This suggested that the initial formation of 1,3,3-trimethyl-2-methyleneindoline **4B** (conjugate base; Fischer's base) is crucial for the reaction; the pK_a in water of **4A** (conjugate acid) was estimated to be ~8.5 (Supporting Information). The [**2c**]/[**2b**] concentration ratio decreased from 99:1 at 50 °C to 10:1 in acetonitrile at 80 °C. The absence of water enhanced the **2c** formation (48%), whereas removing oxygen from the solution had no effect. Higher stoichiometric amounts of the starting

material resulted in slightly higher **2c** yields. When Fischer's base **4B** instead of indolinium **4A** was used without a base, the **2c** yields were high (30%) only at elevated concentrations of **4B** and a higher temperature (80 °C). Cyanine **2c** was formed in higher yields in the presence of a base with **4B**. Interestingly, **2c** also was formed in a low but still significant yield (8%) without indolinium **4A** at full conversion.

Effects of Heptamethine Chain Substituents. We evaluated the truncation of Cy7s substituted at the C3' or C4' positions of the chain with either electron-withdrawing (EWG) or electron-donating (EDG) substituents (Table 2). Only pentamethines **2** substituted in the *meso*-position or unsubstituted trimethine cyanine **3a** were detected as products. The highest yields of **2** were obtained from Cy7, bearing strong electron-withdrawing groups (F or CN) at the C3'-position; a higher reaction temperature enhanced truncation only in the case of **1e**. The yields of **3a** were negligible for **1c** and **1e**. Cy7s **1d** and unsubstituted **1b** provided lower Cy5 yields at both temperatures, but the formation of trimethine **3a** from **1d** was the most efficient (28%). Cy7 substituted in the C4'-position (**1g** and **1h**) did not give Cy5 products in detectable amounts, while **3a** was obtained in a low yield.

Table 2. Effects of Chain Substituents ^a



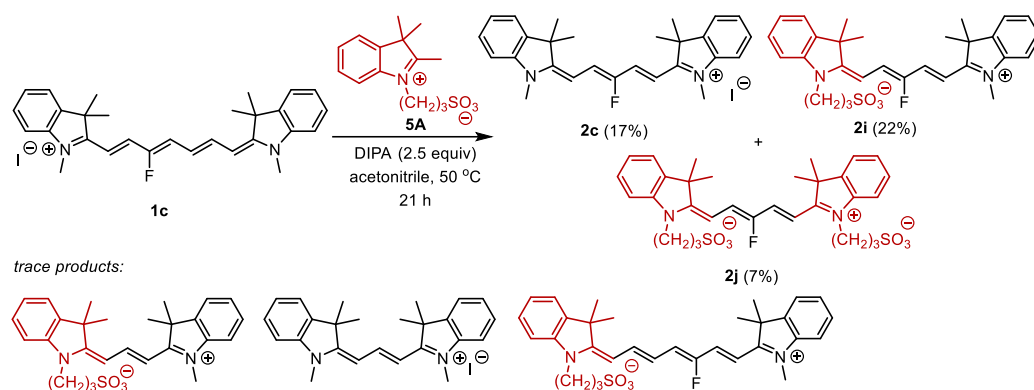
Cy7	R ¹	R ²	conversion of 1 /% at 50 °C or (80 °C)	yield of 2 /% ^b at 50 °C or (80 °C)	yield of 3a /% ^b at 50 °C or (80 °C)
1b	H	H	57 (80)	2b , 15 (15)	1 (4)
1c	F	H	94 (100)	2c , 38 (33) ^c	0.2 (1)
1d	COOCH ₃	H	97 (100)	2d , 16 (15)	28 (22)
1e	CN	H	52 (99)	2e , 15 (30) ^c	1.5 (4)
1f	CH ₃	H	32 (98)	2f , 1 (2)	4 (15)
1g	H	CN	93	2g , 0	0.3
1h	H	COOCH ₃	98	2h , 0	7

^a [**1**] = 72 mM, reaction time = 21 h. Reactions carried out at 50 °C or 80 °C (in the parentheses), iodide as a counteranion is omitted for clarity. The standard deviation from 5 independent measurements was below 2%. ^b HPLC yields (calculated assuming 100% conversion of **1**). ^c Isolated by precipitation.

We evaluated the reaction of **1c** with *N*-substituted indolinium **5** in acetonitrile at 50 °C to follow its incorporation into the products (Scheme 3). All three possible Cy5 derivatives, symmetrical **2c** and **2j**, and non-symmetrical **2i**, were formed in high yields. The formation of the double-ex-

change product **2j** was the least effective as anticipated because it involves at least two subsequent reactions. Trace amounts (<2%) of heptamethine and trimethine cyanines derivatives were also detected, as indicated by the HRMS data (Scheme 3; Figure S17).

Scheme 3. Truncation Reaction Using Different Indolinium Derivatives



Reactions of Cy5 Derivatives. Because Cy5 derivatives are the primary products of the Cy7 truncation, we examined their stability/reactivity under all reaction conditions. Heating Cy5s **2** in the presence of different indolinium derivatives (**4**–**7**) and DIPA only resulted in Cy5 with exchanged terminal indolinium end groups; thus, the pentamethine chain was preserved (Table 3, Table S2). Their relative yields were dependent on the starting material stoichiometry, whereas the quality of the indolinium precursor played only a minor role. When large amounts of Fischer's base **6B** instead of indolinium **6A** were used in the absence of a base, the terminal group exchange was also very efficient. Only traces of Cy3 products were detected (<0.1%, HPLC) in all cases. The presence of an electron-withdrawing group in the *meso*-position was found to be indispensable for the indolinium exchange. Unsubstituted pentamethine derivatives were unreactive under the given conditions.

Truncation Mechanism of 1c. Based on the known Cy7 reactivity^{23–24} and our initial experimental observations, we assumed that the primary reaction step for Cy7 truncation

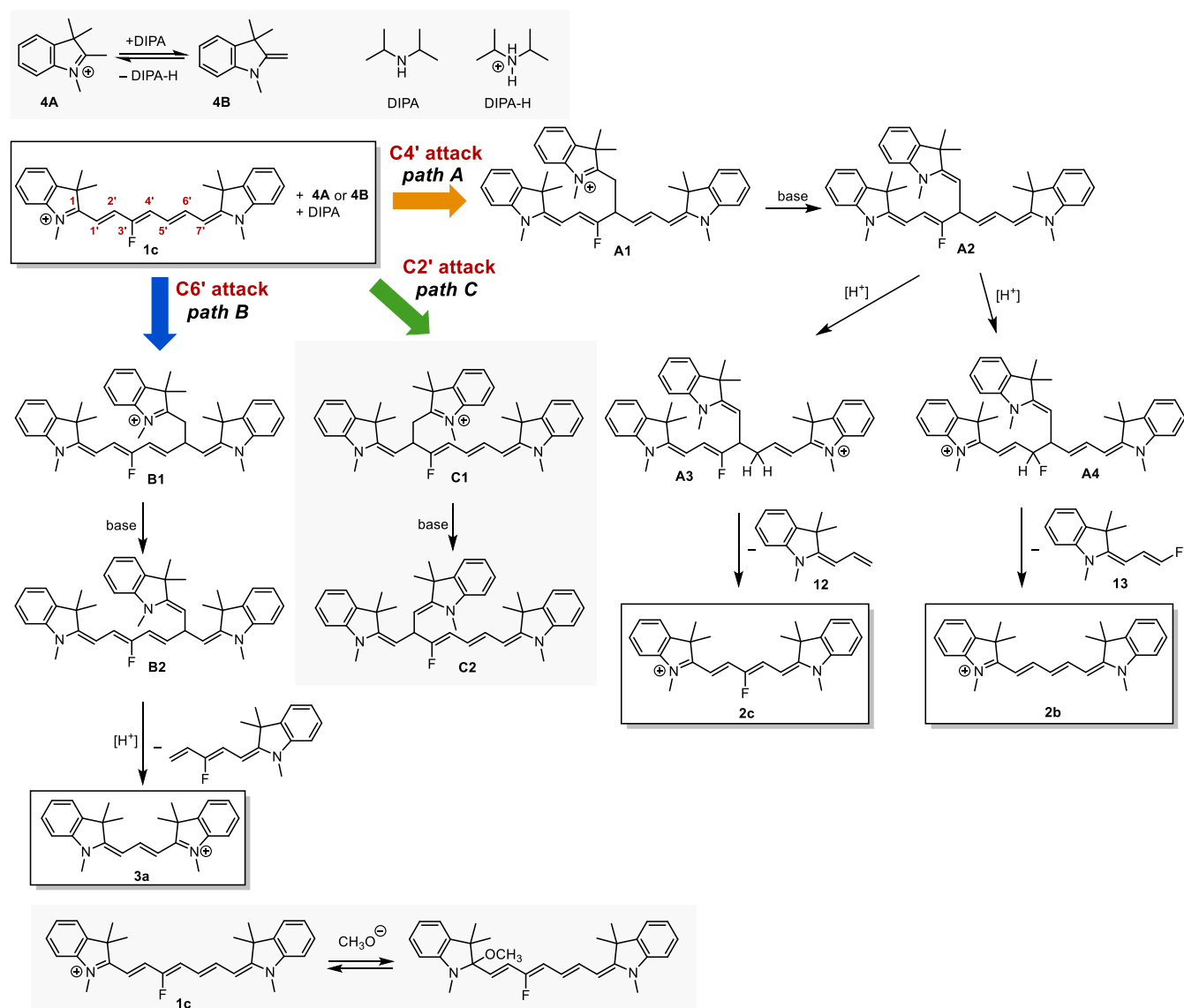
is the nucleophilic addition of an indolinium nucleophile **4B** to the Cy7 polyene chain. Fischer's base **4B** was generated *in situ* in the presence of DIPA from **4A** in all investigated solvents, ethanol, methanol, and acetonitrile (Figures S50 and S51). A strong base was found to be essential for the deprotonation of **4A** ($pK_a = 8.5$) in methanol and acetonitrile solutions (Figures S51 and S52). Three possible electrophilic sites for a non-symmetrical attack of **1c** are the C4', C6', and C2' chain positions to give three charged adducts **A1**, **B1**, and **C1**, respectively (Scheme 4). They can be deprotonated by DIPA to give **A2**, **B2**, and **C2** and subsequently be protonated at various positions to form, for example, **A3** or **A4** from **A2** (*path A*, Scheme 4). A nucleophile could also attack the electrophilic iminium C1 carbon, although this site is sterically hindered (Scheme 4, bottom), while this reaction step does not lead to Cy7 truncation. Indeed, we identified a product of the reversible addition of a strong nucleophile (MeONa) to C1 of **1c** and **2c** at room temperature (Figures S45–49), although no addition was detected when **4B** was used.

Table 3. Reactions of Cyanine Derivatives 2 ^a

2		/equiv ^b	base	conversion/% ^c	[2]:[2-mono]:[2-di] / % ^d
		1	DIPA (2.5 equiv)	59	41:47:10
		5	DIPA (5.5 equiv)	79	21:52:27
		1	DIPA (2.5 equiv)	38	62:31:3
		1	DIPA (2.5 equiv)	69	31:13:0
		1	DIPA (2.5 equiv)	52	48:18:0
		1	DIPA (2.5 equiv)	<1	0
		1	–	71	29:50:18 ^d
		10	–	100	0:13:78 ^e

^a [7] = 36 mM, reaction time = 21 h; n.a. = not applicable, iodide as a counteranion is omitted for clarity. The standard deviation from 5 independent measurements was below 3%. ^b The amount of Het². ^c Reaction conversion. ^d HPLC yields (calculated for the 100% conversion of 2).

Scheme 4. Mechanism of **1c** Truncation in the Presence of **4**



The atmospheric pressure chemical ionization (APCI) HRMS analysis of the crude reaction mixtures of **1c** reaction with **4** (Table 2) revealed the signal at m/z 600.3750 corresponding to $[\text{M}]^+$ of the expected intermediates **A1**, **B1**, and **C1** or $[\text{M}+\text{H}]^+$ of **A2**, **B2**, and **C2** (Scheme 4, Figure S10). Interestingly, electrospray ionization (ESI) HRMS of the same reaction mixture gave the signals at m/z 598.3580 and 596.3454, which would correspond to $[\text{M}-\text{H}]^+$ and $[\text{M}-3\text{H}]^+$ of intermediates **A2**, **B2**, and **C2**, respectively (Figure S11). Electrochemical oxidation occurring in the electrospray emitter during mass analysis⁴¹ is probably the reason for different ion signals in the ESI⁺, which was also reported, for example, for bisindolylmethanes⁴² or dihydropyridines.⁴³ Analogous intermediates were also identified in the reactions of other heptamethine derivatives **1** (Table 2) using the APCI⁺ and ESI⁺ analyses (Table S3). All attempts to isolate the adducts were unsuccessful, probably due to their rapid decomposition during the isolation procedures.

To follow *path A*, adduct **A2**, protonated at the C5' position, releases an allylideneindoline fragment **12** to give the

truncated **2c** derivative as the major product. Electron-rich butadienyl species, probably formed during this transformation, are reported to be very reactive.^{27,44} They could attack an electron-deficient molecule, such as starting **1c**, to form chain-extended nonamethine cyanines. Indeed, a trace mass signal corresponding to fluorinated nonamethine derivative was detected by ESI-HRMS (Figure S11). On the other hand, protonation of **A2** at the C3' position and subsequent release of a fluoroallylidene fragment **13** leads to the formation of unsubstituted **2b**, observed as a minor product. The **2b** yield increased at elevated temperatures (50–80 °C), which could be related to different kinetic factors.

Adducts **B2** and **C2** (*paths B* and *C*, Scheme 4) can produce **Cy3 3a** (but not **2c** or **2b**) upon protonation and the release of the corresponding indoline fragments. As **2c** and **2b** are the major observed products, the formation of the **B2** and **C2** intermediates must be inefficient.

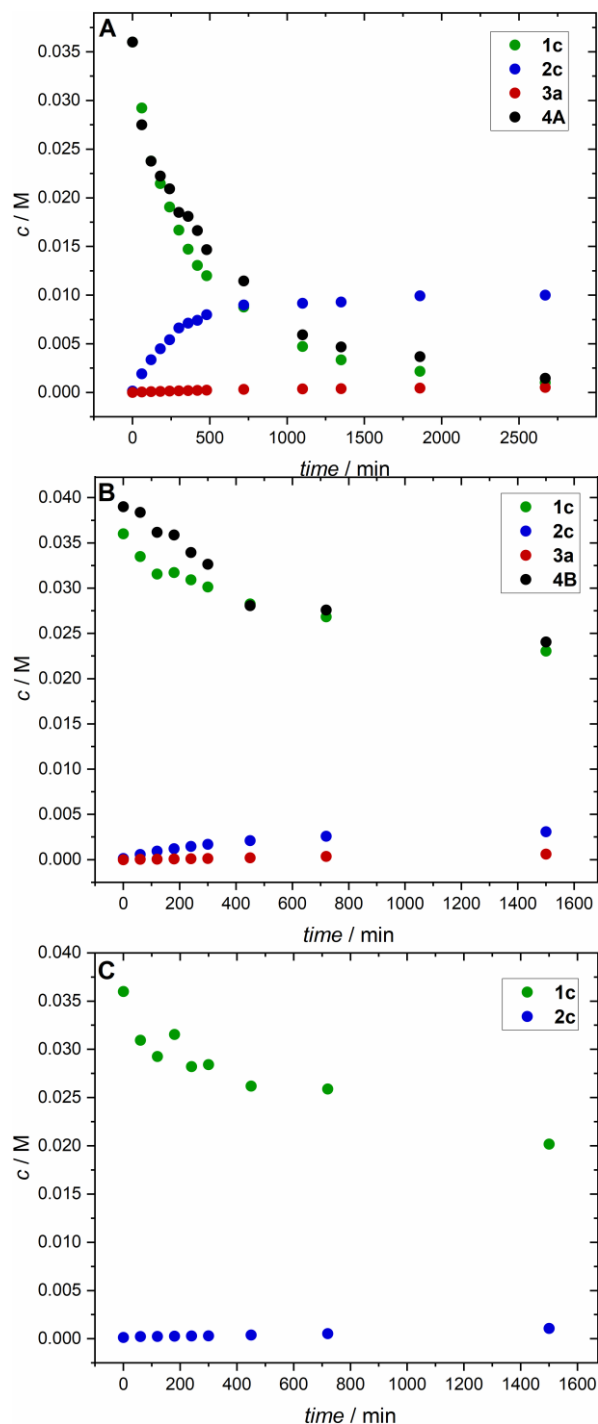
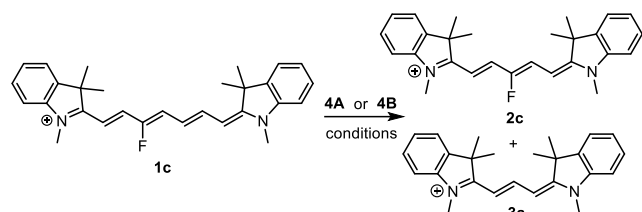


Figure 1. Concentration profiles for the reactions of **1c**. Reaction conditions: (a) **1c** (36 mM), **4A** (36 mM), DIPA (9 mM) in acetonitrile (10 mL) stirred at 50 °C; (b) **1c** (36 mM) and **4B** (36 mM) in acetonitrile (10 mL) stirred at 50 °C; (c) **1c** (36 mM) and DIPA (9 mM) in acetonitrile (10 mL) stirred at 50 °C.

To understand the role of a base (DIPA) in the truncation process, we investigated the reaction kinetics of **1c** in acetonitrile to give products **2c** and **3a** under three different conditions: in the presence of (a) DIPA and indolinium salt **4A**, (b) Fischer's base **4B** only (no DIPA), and (c) DIPA only (no **4**) (Figure 1). The most efficient product **2c** formation but inefficient **3a** formation was observed under the conditions (a). The kinetic data were fitted to a second-order reaction of **1c** + **4A** → **2c** (Figure S3), and the rate constant of the **2c** formation was essentially the same in methanol ($(1.77 \pm 0.1) \times 10^{-3} \text{ M}^{-1} \text{ s}^{-1}$) and acetonitrile ($(1.70 \pm 0.1) \times 10^{-3} \text{ M}^{-1} \text{ s}^{-1}$). The absence of DIPA in (b) did not stop the truncation process; the reaction was only slowed down with an estimated rate constant of the **2c** formation of $(2.0 \pm 0.2) \times 10^{-4} \text{ M}^{-1} \text{ s}^{-1}$ in acetonitrile (when Fischer's base **4B** was used in the absence of a base, the truncation was always less efficient, Table 1). The reaction (c) led to an insignificant conversion of the starting material to give **2c** with a reaction rate constant of $(5.7 \pm 0.7) \times 10^{-6} \text{ s}^{-1}$ in acetonitrile; the formation of **2c** was negligible. We conclude that DIPA must be productively involved in the **4A/4B** conversion and subsequent acid-base equilibria.

Quantum-Chemical Calculation: Energies vs. Free Energies. The above-suggested mechanism (Scheme 4) poses multiple challenges for the theoretical treatment. First, the catalytic steps involve changes in the molecularity; thus, we can expect a significant contribution of entropic and solvent effects. The proper modeling of the entropic and solvent effects is a matter of heated discussions, mainly revolving around the coverage of translational entropy.⁴⁵⁻⁴⁹

There is extensive empirical evidence that the full inclusion of the translational entropy with most of standard density functional theory (DFT) functionals leads to the overestimation of activation energies by ~0.3 eV for bimolecular transition states.⁵⁰ Some researchers have suggested that the effect of translational entropy on free energy should be ignored entirely in solutions.⁵¹⁻⁵² However, this approach is hard to justify. The experimental data in organic chemistry were also reproduced with the concepts based on the free volume that effectively reduces the contribution of translational entropy.⁴⁸ A similar effect was achieved within the explicit scaling approaches, with only a fraction of the calculated translational entropy included.⁴⁹ As an example, Singleton has successfully applied the $\Delta G_{50\%}$ method for modeling the Morita–Baylis–Hillman reaction with similar acid-base catalytic cycles considered in this work.⁴⁵ Again, we see a minimal theoretical foundation for the latter treatment, however well the method works in practice. Sunoy and co-workers argued that the free energy surface matching the experimental data for the same reaction could be obtained with no translational entropy scaling or any other *ad hoc* treatment, providing that high-level electronic structure methods are used and solvent entropy is adequately described.⁴⁷ Perrin and co-workers then strongly support the view that the full contribution of translational entropy from Sackur–Tetrode equation should be included.⁴⁶ The results presented here are in line with their conclusions.

The role of the entropic effects in our systems is demonstrated on the **1c** truncation through the addition of **4B** to **C4'** (*path A*, Scheme 4). The electronic energy profile (i.e.,

the energetics ignoring thermal and entropic contributions) (red line, Figure 2) indicates that the main products should be two intermediates, **A1** and **A2**, whereas the final product **2c** is destabilized by 0.79 eV against the lowest-energy structure. The highest calculated activation barrier is 0.74 eV. From a naïve perspective, one would expect that the reaction leading to the trimolecular complex **A2** mixed with the **A1** adduct is relatively fast.

The *Gibbs free energies* (orange line, Figure 2) differ significantly from the electronic energies thanks to entropic effects (green line, Figure 2). The calculated free energy profile perfectly agrees with the experimental observations, including the observed products and the reaction kinetics. The electronic energies were calculated with a high-level *ab initio* DLPNO-CCSD(T)/cc-pVTZ method (Figures 2 and S57), and no correction for the translational entropy was needed (see SI for further discussion). We can compare these results with the free energies evaluated at the density functional level (PBE0/def2-TZVP/D3BJ, Figure S54). While the entropy addition correctly disfavors the intermediates, the calculated barriers at the DFT level are, in contrast to CCSD(T) results, too large to expect the reaction to occur within tens of hours. The $\Delta G_{50\%}$ correction results are then consistent with the experiment (Figure S54). Our results thus seem to support the views of Perrin and Sunoy mentioned above;⁴⁶⁻⁴⁷ that is, no further corrections to the entropic terms are needed when an appropriate level of theory is used. At the same time, when common DFT calculations are used, the scaling approaches represent a pragmatic approach to model catalytic reactions, even if they are based on error cancellation.

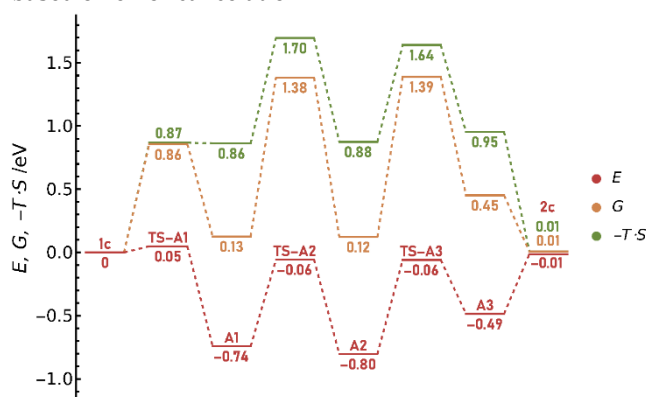


Figure 2. Calculated electronic (red) and Gibbs (orange) free energy profiles and entropic contributions (green) at 358 K for a path following the attack of **4B** to C4' of **1c** (Scheme 4, *path A*). “TS” stands for the corresponding transition state. The single point electronic energies were calculated at the DLPNO-CCSD(T)/cc-pVTZ level in ethanol within the polarizable continuum model (PCM). Thermal corrections were evaluated in the gas phase at the PBE0/def2-TZVP level with the D3BJ dispersion correction. The inclusion of solvation at the DLPNO-CCSD(T) level is described in the methodology section (Supporting Information). The structures were optimized at the same level as the frequency calculations.

Further effects influencing the Gibbs free energy profile and reaction rates were considered. The reaction rate for a path following the attack of **4B** to **1c** is slightly increased

thanks to hydrogen tunneling, which causes a decrease in the apparent activation energies. The accelerating effect of hydrogen tunneling occurs because the rate-limiting step is proton transfer. The corrections were calculated according to Bell's method.⁵³ For deprotonation by DIPA (**A1**→**A2**), the decrease in the activation Gibbs free energy by a quantum tunneling correction is up to 0.08 eV, whereas protonation by DIPA-H (**A2**→**A3**) gives the Gibbs free energy lowered by 0.04 eV. We also found that deprotonation of **A1** by DIPA can occur through four different transition states with almost identical energies. This leads to further decreased activation entropy, resulting in the activation Gibbs free energy drop by 0.04 eV at 358 K. All these effects are included in the energetic profiles in Figures 2 and 3.

In the presence of DIPA, **4A** is deprotonated to **4B**, which is accompanied by a decrease in Gibbs free energy by 0.17 eV, implying an equilibrium constant of $K = 260$ (at the DLPNO-CCSD(T)/cc-pVTZ level in ethanol with thermal corrections from the PBE0/def2-TZVP/D3BJ level using a standard state of 1M at 358 K). The C4' attack of **4B** to **1c** (leading to **A1**) has the lowest transition state (Figure 3) when compared to the C2' and C6' attacks (giving **C1** and **B1**, respectively). Moreover, **A1** has the lowest free energy among the three resulting adducts **A1**, **B1**, and **C1**, with the other two being positioned about 0.2 eV higher. Thus, the C4' attack is both kinetically and thermodynamically preferred over the C2' and C6' attacks, as supported by the experimental results (see above). The C4' adduct has the lowest activation Gibbs free energy for the subsequent deprotonation step with DIPA (related to the starting **1c**) to form **A2**. This deprotonated product is then the most stable compared to the other two concurrent deprotonated products **B2** and **C2**, obtained from the C6' and C2' adducts, respectively.

From this point on, we only discuss the calculation of the C4' attack pathway. The pathway to the truncated fluorinated **2c** product leads through the protonation of **A2** at the C5' carbon (here, by DIPA-H), forming **A3**, which then decomposes to **2c**. These steps are energetically more favorable than the C3' protonation pathway, which requires free energy higher by 0.36 eV to cross the activation barrier. This pathway then leads to an intermediate **A4**, which is by 0.12 eV less stable than **A3**. The final product is then **2b**, which has almost the same relative energy as **2c**. The higher activation energy for the C3' protonation corresponds to the observed temperature dependence of the **2b/2c** product ratio discussed above. As both species have the same free energy, their yields must be kinetically controlled. Secondary (DIPA) or tertiary (DIPEA) amines or **4B** can serve as bases. When only **4B** is used (i.e., no DIPA or DIPEA), the Gibbs free energy change for deprotonation of **A1** to give **A2** in the presence of **4B** is 0.18 eV. A comparison of the value for deprotonation with DIPA as a base (0.01 eV) provides one of the possible reasons for the lower truncation yields when **4B** is used alone.

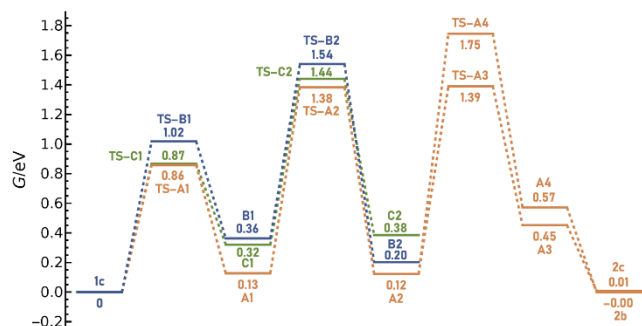
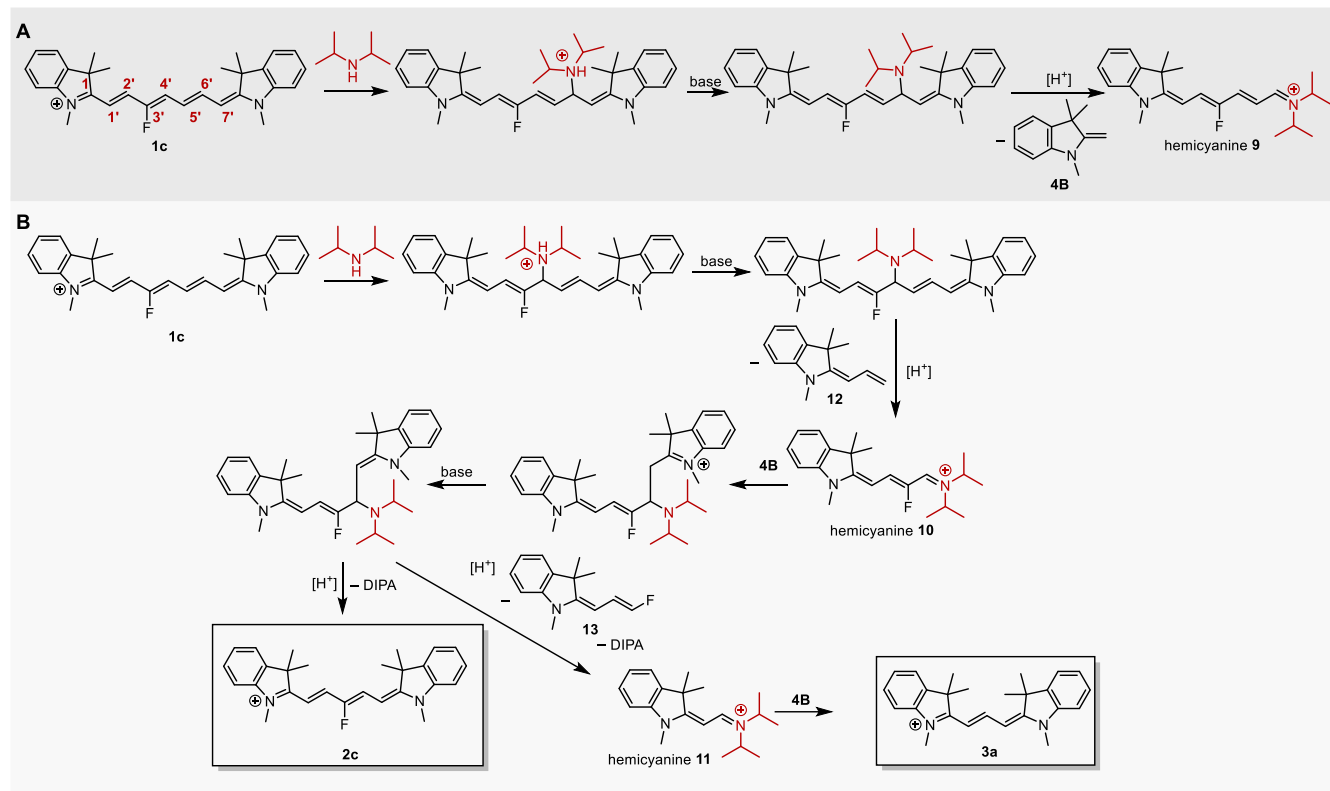


Figure 3. Gibbs free energies of the addition of **4B** to **1c** (Scheme 4) in ethanol at the standard state of 1 M at 358 K. The structures were optimized in the gas phase at the PBE0/def2-TZVP level with the D3BJ dispersion correction. Single points energies were calculated at the DLPNO-CCSD(T)/cc-pVTZ level. Frequency calculations were conducted at the same level as optimization with the inclusion of solvation (at the DLPNO-CCSD(T)/cc-pVTZ level) described in the methodology (Supporting Information).

Scheme 5. Truncation of **1c** with DIPA



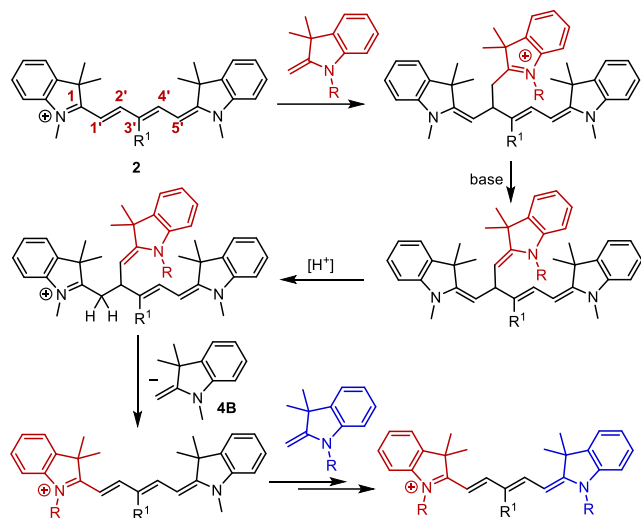
Reactions of Other Cy7 Derivatives. The presence of an electron-withdrawing group (F, CN, COOMe) in **1** or the absence of substituents are favorable for the formation of **2**, whereas no truncation product was observed for **1f** (3'-methyl derivative; Table 2). This is most likely related to the chain activation for nucleophilic attack. On the other hand, any substituent in the C4' position of **1** (Table 2) has a detrimental effect on truncation, which may, at least partially, be associated with a higher steric demand at the C4' position. Indeed, the calculated activation free energy of **4B** attack to the C4' of **1g** is 0.96 eV, which is higher than for **1c** by 0.1 eV. The resulting adduct **D1** is less energetically stable than the **A1** adduct by 0.28 eV (Figure S56).

Truncation with Secondary Amine. The reaction of **1c** in the absence of Fischer's base but in the presence of a secondary amine (DIPA) still leads to truncation, although with very low yields (Table 1). Therefore, we considered the

reaction mechanism in which DIPA acts as a nucleophile attacking the cyanine chain. The addition to the C6' position resulted in the formation of hemicyanine **9** and the release of product **4B**, the masses of which were confirmed by HRMS (Scheme 5A, Figure S26). The released **4B** could subsequently attack the starting **1c** to give **2c** via the above-described mechanism (Scheme 4). The addition of DIPA to C4' would provide hemicyanine **10**, which could lead to **2c** in the presence of the released indolinium (Scheme 5B). As shown above (Figure 1c), this is a considerably slower process than the addition of **4A** or **4B** to **1c**. However, as the presence of a tertiary amine (DIPEA) leads to the same results as DIPA (Table 1), indolinium could also be generated by an alternative degradation pathway, which we did not investigate further. In agreement with the experimental data, the calculation of the pathway shown in Scheme 5B pro-

vided high Gibbs free energy values for the suggested adduct intermediates, which indicates a low probability of this reaction step (Figure S57).

Scheme 6. Exchange of Terminal Heterocycles in 2



Exchange of Terminal Heterocycles in Cy5. Pentamethine cyanines do not undergo truncation to give Cy3 derivatives under the studied conditions. However, the exchange of heterocyclic ends was observed in Cy5s substituted with EWG at the C3' position (Table 3). The presence of an EWG in the polyene chain increases its electrophilicity, making the nucleophilic attack of indolinium more probable. The mechanism involving several steps identical to those in the Cy7→Cy5 truncation is shown in Scheme 6. The reaction proceeds efficiently with Fischer's base in the absence of a base (the reaction with **6B**, Table 3); therefore, the primary and probably only productive role of DIPA in all other processes is the deprotonation of the starting indolinium salt.

Conclusions

We found that heptamethine cyanines (Cy7) can be cleaved in various positions of the polymethine chain and converted to pentamethine cyanines (Cy5) in the presence of heterocyclic nucleophiles, such as an indolinium salt, at elevated temperatures in both protic and aprotic solvents. This truncation reaction is efficient and generally applicable to different Cy7 derivatives and nucleophiles.

Our mechanistic analysis revealed that truncation is strongly affected by the quality of nucleophiles and reaction conditions and that electron-withdrawing groups significantly enhance the reactivity of the polyene chain. The resulting Cy5 products do not undergo chain shortening under the given conditions, but instead, they exhibit the exchange of heterocyclic end groups via the attack of a nucleophile to the C2' position. All suggested mechanisms were supported by computational analysis, providing the activation barriers consistent with the experimentally observed

rates and amounts of identified intermediates. This work expands the knowledge of the reactivity of cyanine dyes and opens the pathways to synthesize their new derivatives.

Our work can also contribute to the discussion on the role of computational chemistry in the revealing mechanisms of homogeneous catalytic reactions. While Singleton has expressed a rather skeptical view on the real importance of the *ab initio* computational predictions,⁴⁵ Harvey and his co-workers responded more optimistically.⁴⁷ Our present case supports Harvey's views on the role of computational chemistry and the technology that should be utilized. The truncation reaction mechanisms discussed in this work were not suggested based on computational studies; instead, they were proposed through intuition and experience of organic chemists. Yet computational techniques can distinguish between different pathways and support the quantitatively consistent mechanism with the experimental observations. Our work suggests that computational techniques beyond the density functional theory family represent a safe choice. The coupled cluster calculations can be efficiently performed with locally correlated techniques for medium-sized molecules, and this technique provides a quantitative treatment of catalytic reactions.

ASSOCIATED CONTENT

Supporting Information. Materials and methods; synthesis; NMR, absorption, and emission data; quantum-chemical calculations. This material is available free of charge via the Internet at <http://pubs.acs.org>.

AUTHOR INFORMATION

Corresponding Authors

* Petr Slavíček: Petr.Slavicek@vscht.cz; Petr Klán: klan@sci.muni.cz

Notes

The authors declare no competing financial interest.

ACKNOWLEDGMENT

The authors thank the Czech Science Foundation (P.K.: GA23-05111S, and P.S. and J.F.: GA23-07066S) and the RECETOX Research Infrastructure (No. LM2023069), financed by the Czech Ministry of Education, Youth and Sports, and the Operational Programme Research, Development for supportive background. This project was also supported by the European Union's Horizon 2020 Research and Innovation Programme under grant agreement No. 857560 (P.K.). The authors also acknowledge the support from the National Infrastructure for Chemical Biology (CZ-OPENSREEN, LM2023052; P.K.). This publication reflects only the author's view and the European Commission is not responsible for any use that may be made of the information it contains. P.S. was supported by the project "The Energy Conversion and Storage", funded as a project No.

References

1. Ilina, K.; Henary, M., Cyanine dyes containing quinoline moieties: history, synthesis, optical properties, and applications. *Chem. Eur. J.* **2021**, *27*, 4230-4248.
2. Gorka, A. P.; Nani, R. R.; Schnermann, M. J., Cyanine polyene reactivity: scope and biomedical applications. *Org. Biomol. Chem.* **2015**, *13*, 7584-7598.
3. Njiojob, C. N.; Owens, E. A.; Narayana, L.; Hyun, H.; Choi, H. S.; Henary, M., Tailored near-infrared contrast agents for image guided surgery. *J. Med. Chem.* **2015**, *58*, 2845-2854.
4. Shi, C.; Wu, J. B.; Pan, D., Review on near-infrared heptamethine cyanine dyes as theranostic agents for tumor imaging, targeting, and photodynamic therapy. *J. Biochem. Opt.* **2016**, *21*, 050901.
5. Choi, H. S.; Nasr, K.; Alyabyev, S.; Feith, D.; Lee, J. H.; Kim, S. H.; Ashitate, Y.; Hyun, H.; Patonay, G.; Strekowski, L.; Henary, M.; Frangioni, J. V., Synthesis and In Vivo Fate of Zwitterionic Near-Infrared Fluorophores. *Angew. Chem. Int. Ed.* **2011**, *50*, 6258-6263.
6. Choi, H. S.; Gibbs, S. L.; Lee, J. H.; Kim, S. H.; Ashitate, Y.; Liu, F.; Hyun, H.; Park, G.; Xie, Y.; Bae, S.; Henary, M.; Frangioni, J. V., Targeted zwitterionic near-infrared fluorophores for improved optical imaging. *Nat. Biotechnol.* **2013**, *31*, 148-153.
7. Owens, E. A.; Hyun, H.; Tawney, J. G.; Choi, H. S.; Henary, M., Correlating molecular character of NIR imaging agents with tissue-specific uptake. *J. Med. Chem.* **2015**, *58*, 4348-4356.
8. Hyun, H.; Park, M. H.; Owens, E. A.; Wada, H.; Henary, M.; Handgraaf, H. J.; Vahrmeijer, A. L.; Frangioni, J. V.; Choi, H. S., Structure-inherent targeting of near-infrared fluorophores for parathyroid and thyroid gland imaging. *Nat. Med.* **2015**, *21*, 192-197.
9. Kiyose, K.; Aizawa, S.; Sasaki, E.; Kojima, H.; Hanaoka, K.; Terai, T.; Urano, Y.; Nagano, T., Molecular design strategies for near-infrared ratiometric fluorescent probes based on the unique spectral properties of aminocyanines. *Chem. Eur. J.* **2009**, *15*, 9191-9200.
10. Salon, J.; Ska, E. W.; Raszkievicz, A.; Patonay, G.; Strekowski, L., Synthesis of benz[e]indolium heptamethine cyanines containing C-substituents at the central portion of the heptamethine moiety. *J. Heterocycl. Chem.* **2005**, *42*, 959-961.
11. Stackova, L.; Muchova, E.; Russo, M.; Slavicek, P.; Stacko, P.; Klan, P., Deciphering the structure-property relations in substituted heptamethine cyanines. *J. Org. Chem.* **2020**, *85*, 9776-9790.
12. Stackova, L.; Stacko, P.; Klan, P., Approach to a substituted heptamethine cyanine chain by the ring opening of zincke salts. *J. Am. Chem. Soc.* **2019**, *141*, 7155-7162.
13. Han, J.; Engler, A.; Qi, J.; Tung, C.-H., Ultra pseudo-Stokes shift near infrared dyes based on energy transfer. *Tetrahedron Lett.* **2013**, *54*, 502-505.
14. Miao, Q.; Ye, D. C.; Wiraja, C.; Zhang, J.; Ning, X.; Xu, C.; Pu, K., Near-infrared fluorescent molecular probe for sensitive imaging of keloid. *Angew. Chem. Int. Ed.* **2018**, *57*, 1256-1260.
15. Cai, S.; Liu, C.; Jiao, X.; He, S.; Zhao, L.; Zeng, X., A lysosome-targeted near-infrared fluorescent probe for imaging of acid phosphatase in living cells. *Org. Biomol. Chem.* **2020**, *18*, 1148-1154.
16. Zhu, D.; Li, G.; Xue, L.; Jiang, H., Development of ratiometric near-infrared fluorescent probes using analyte-specific cleavage of carbamate. *Org. Biomol. Chem.* **2013**, *11*, 4577-4580.
17. Lee, H.; Mason, J. C.; Achilefu, S., Heptamethine cyanine dyes with a robust C-C bond at the central position of the chromophore. *J. Org. Chem.* **2006**, *71*, 7862-7865.
18. Young, D. N.; Detty, M. R., Hydrolysis studies of chalcogenopyrylium trimethine dyes. 1. Product studies in alkaline solution (pH \geq 8) under anaerobic and aerobic conditions. *J. Org. Chem.* **1997**, *62*, 4692-4700.
19. Gosi, M.; Marepu, N.; Sunandamma, Y., Cyanine-based fluorescent probe for cyanide ion detection. *J. Fluoresc.* **2021**, *31*, 1409-1415.
20. Mahapatra, A. K.; Maiti, K.; Maji, R.; Manna, S. K.; Mondal, S.; Ali, S. S.; Manna, S., Ratiometric fluorescent and chromogenic chemodosimeter for cyanide detection in water and its application in bioimaging. *RSC Adv.* **2015**, *5*, 24274-24280.
21. Niu, H.-T.; Jiang, X.; He, J.; Cheng, J.-P., Cyanine dye-based chromofluorescent probe for highly sensitive and selective detection of cyanide in water. *Tetrahedron Lett.* **2009**, *50*, 6668-6671.
22. Kundu, K.; Knight, S. F.; Willett, N.; Lee, S.; Taylor, W. R.; Murthy, N., Hydrocyanines: a class of fluorescent sensors that can image reactive oxygen species in cell culture, tissue, and in vivo. *Angew. Chem. Int. Ed.* **2009**, *48*, 299.
23. Vompe, A.; Ivanova, L.; Meskhi, L.; Monich, N.; Raikhina, R., Synthesis of pseudobases of polymethine dyes and their reactions. *Zh. Org. Khim.* **1985**, *21*, 584-594.
24. Nikolajewski, H.; Dähne, S.; Hirsch, B.; Jauer, E. A., Aminolysis of C-C linkages. *Angew. Chem. Int. Ed.* **1966**, *5*, 1044-1044.
25. Alías, S.; Andreu, R.; Blesa, M. J.; Cerdán, M. A.; Franco, S.; Garín, J.; López, C.; Orduna, J.; Sanz, J.; Alicante, R., Iminium salts of ω -dithiafulvenylpolyenals: an easy entry to the corresponding aldehydes and doubly proaromatic nonlinear optic-phores. *J. Org. Chem.* **2008**, *73*, 5890-5898.
26. Alías, S.; Andreu, R.; Cerdán, M. A.; Franco, S.; Garín, J.; Orduna, J.; Romero, P.; Villacampa, B., Synthesis, characterization and optical properties of merocyanines derived from malononitrile dimer. *Tetrahedron Lett.* **2007**, *48*, 6539-6542.
27. Khan, M. N.; Fleury, J.-P.; Baumlin, P.; Hubschwerlen, C., A new route to trinuclear carbocyanines. *Tetrahedron* **1985**, *41*, 5341-5345.
28. Eiermann, M.; Stowasser, B.; Hafner, K.; Bierwirth, K.; Frank, A.; Lerch, A.; Reußwig, J., Synthesis and properties of vinylogous 6-(cyclopentadienyl)pentafulvenes. *Chem. Ber.* **1990**, *123*, 1421-1431.
29. Gorka, A. P.; Nani, R. R.; Schnermann, M. J., Harnessing cyanine Rreactivity for optical imaging and drug delivery. *Acc. Chem. Res.* **2018**, *51*, 3226-3235.
30. Jradi, F. M.; Lavis, L. D., Chemistry of photosensitive Ffluorophores for single-molecule localization microscopy. *ACS Chem. Biol.* **2019**, *14*, 1077-1090.
31. Bandi, V. G.; Luciano, M. P.; Saccomano, M.; Patel, N. L.; Bischof, T. S.; Lingg, J. G. P.; Tsrunchev, P. T.; Nix, M. N.; Ruehle, B.; Sanders, C.; Riffle, L.; Robinson, C. M.; Difilippantonio, S;

- Kalen, J. D.; Resch-Genger, U.; Ivanic, J.; Bruns, O. T.; Schnermann, M. J., Targeted multicolor in vivo imaging over 1,000 nm enabled by nonamethine cyanines. *Nat. Methods* **2022**, *19*, 353-358.
32. Matikonda, S. S.; Helmerich, D. A.; Meub, M.; Beliu, G.; Kollmannsberger, P.; Greer, A.; Sauer, M.; Schnermann, M. J., Defining the basis of cyanine phototruncation enables a new approach to single-molecule localization microscopy. *ACS Cent. Sci.* **2021**, *7*, 1144-1155.
33. Helmerich, D. A.; Beliu, G.; Matikonda, S. S.; Schnermann, M. J.; Sauer, M., Photoblueing of organic dyes can cause artifacts in super-resolution microscopy. *Nat. Methods* **2021**, *18*, 253-257.
34. Fukushima, H.; Matikonda, S. S.; Usama, S. M.; Furusawa, A.; Kato, T.; Štacková, L.; Klán, P.; Kobayashi, H.; Schnermann, M. J., Cyanine phototruncation enables spatiotemporal cell labeling. *J. Am. Chem. Soc.* **2022**, *144*, 11075-11080.
35. Stone, M. B.; Veatch, S. L., Far-red organic fluorophores contain a fluorescent impurity. *ChemPhysChem* **2014**, *15*, 2240-2246.
36. Kwok, S. J. J.; Choi, M.; Bhayana, B.; Zhang, X.; Ran, C.; Yun, S.-H., Two-photon excited photoconversion of cyanine-based dyes. *Sci. Rep.* **2016**, *6*, 23866.
37. Cho, Y.; An, H. J.; Kim, T.; Lee, C.; Lee, N. K., Mechanism of cyanine5 to cyanine3 photoconversion and its application for high-density single-particle tracking in a living cell. *J. Am. Chem. Soc.* **2021**, *143*, 14125-14135.
38. Flanagan, J. H.; Khan, S. H.; Menchen, S.; Soper, S. A.; Hammer, R. P., Functionalized tricarbocyanine dyes as near-infrared fluorescent probes for biomolecules. *Bioconjugate Chem.* **1997**, *8*, 751-756.
39. Van Der Wal, S.; Kuil, J.; Valentijn, A. R. P.; Van Leeuwen, F. W., Synthesis and systematic evaluation of symmetric sulfonated centrally CC bonded cyanine near-infrared dyes for protein labelling. *Dyes Pigm.* **2016**, *132*, 7-19.
40. Mizrahi, D. M.; Ziv-Polat, O.; Perlstein, B.; Gluz, E.; Margel, S., Synthesis, fluorescence and biodistribution of a bone-targeted near-infrared conjugate. *Eur. J. Med. Chem.* **2011**, *46*, 5175-5183.
41. Mora, J. F. d. l.; Van Berkel, G. J.; Enke, C. G.; Cole, R. B.; Martinez-Sanchez, M.; Fenn, J. B., Electrochemical processes in electrospray ionization mass spectrometry. *J. Mass. Spectrom.* **2000**, *35*, 939-952.
42. Xu, X.; He, G.; Xu, X.; Wu, Z.; Cai, T., Investigation of the electrochemical oxidation of 2, 3'-bisindolylmethanes in positive-ion electrospray ionization mass spectrometry. *RSC Adv.* **2019**, *9*, 10727-10732.
43. Chai, Y.; Sun, H.; Wan, J.; Pan, Y.; Sun, C., Hydride abstraction in positive-ion electrospray interface: oxidation of 1, 4-dihydropyridines in electrospray ionization mass spectrometry. *Analyst* **2011**, *136*, 4667-4669.
44. Hubschwerlen, C.; Fleury, J.-P., Diènamines hétérocycliques—II: Condensation de la base de fischer sur des aldéhydes aliphatiques saturés. Formation d'azatriènes. *Tetrahedron* **1977**, *33*, 761-765.
45. Plata, R. E.; Singleton, D. A., A case study of the mechanism of alcohol-mediated Morita Baylis-Hillman reactions. The importance of experimental observations. *J. Am. Chem. Soc.* **2015**, *137*, 3811-3826.
46. Harvey, J. N.; Himo, F.; Maseras, F.; Perrin, L., Scope and challenge of computational methods for studying mechanism and reactivity in homogeneous catalysis. *Acc Catalysis* **2019**, *9*, 6803-6813.
47. Liu, Z.; Patel, C.; Harvey, J. N.; Sunoj, R. B., Mechanism and reactivity in the Morita-Baylis-Hillman reaction: the challenge of accurate computations. *Phys. Chem. Chem. Phys.* **2017**, *19*, 30647-30657.
48. Mammen, M.; Shakhnovich, E. I.; Deutch, J. M.; Whitesides, G. M., Estimating the entropic cost of self-assembly of multiparticle hydrogen-bonded aggregates based on the cyanuric acid melamine lattice. *J. Org. Chem.* **1998**, *63*, 3821-3830.
49. Cooper, J.; Ziegler, T., A density functional study of S_N2 substitution at square-planar platinum (II) complexes. *Inorg. Chem.* **2002**, *41*, 6614-6622.
50. Liu, S.-C.; Zhu, X.-R.; Liu, D.-Y.; Fang, D.-C., DFT calculations on the solvation systems--solvation energy, dispersion energy and entropy. *Phys. Chem. Chem. Phys.* **2022**.
51. Dub, P. A.; Poli, R., A computational study of solution equilibria of platinum-based ethylene hydroamination catalytic species including solvation and counterion effects: Proper treatment of the free energy of solvation. *J. Mol. Catal. A Chem.* **2010**, *324*, 89-96.
52. Tamura, H.; Yamazaki, H.; Sato, H.; Sakaki, S., Iridium-catalyzed borylation of benzene with diboron. Theoretical elucidation of catalytic cycle including unusual iridium (V) intermediate. *J. Am. Chem. Soc.* **2003**, *125*, 16114-16126.
53. Caldin, E. F., Tunneling in proton-transfer reactions in solution. *Chem. Rev.* **1969**, *69*, 135-156.